



Research Article

Impedance testing of porous Si_3N_4 scaffolds for skeletal implant applications



Serdar Onat Akbulut¹ · Hamed Ghorbanpoor² · Betül Özbek İpteç³ · Adrian Butterworth⁴ · Gamze Avcioglu³ · Leyla Didem Kozacı³ · Gülsüm Topateş¹ · Damion K. Corrigan⁴ · Hüseyin Avcı^{5,6} · Fatma D. Güzel²

Received: 28 November 2019 / Accepted: 11 March 2020 / Published online: 6 April 2020
© The Author(s) 2020 **OPEN**

Abstract

Si_3N_4 ceramics show excellent characteristics of mechanical and chemical resistance in combination with good biocompatibility, antibacterial property and radiolucency. Therefore, they are intensively studied as structural materials in skeletal implant applications. Despite their attractive properties, there are limited data in the field about in vitro studies of cellular growth on ceramic implant materials. In this study, the growth of bone cells was investigated on porous silicon nitride (Si_3N_4) ceramic implant by using electrochemical impedance spectroscopy (EIS). Partial sintering was performed at 1700 °C with limited amount of sintering additive for the production of porous Si_3N_4 scaffolds. All samples were then sterilized by using ethylene oxide followed by culturing MG-63 osteosarcoma cells on the substrates for in vitro assays. At 20 and 36 h, EIS was performed and results demonstrated that magnitude of the impedance as a result of the changes in the culture medium increased after incubation with osteosarcoma cells. The changes are attributed to the cellular uptake of charged molecules from the medium. Si_3N_4 samples appear to show large impedance magnitude changes, especially between 100 and 1 Hz. Impedance changes were also correlated with WST-1 measurements (36 h) and DAPI results.

Keywords Electrochemical impedance spectroscopy · Cellular attachment · Bone implant · Si_3N_4

1 Introduction

Si_3N_4 ceramics are non-oxide technical ceramics that have been used in various applications due to its advantageous combination of chemical, thermal, tribological, and mechanical properties [1–4]. Beside these unique properties, the possible usability of Si_3N_4 as a bone substitute or an implant was proven with various studies [5–7]. This is due to the fact that the surface of the Si_3N_4 ceramics has a unique property which helps to increase the metabolic activity of osteoblast cells; this results in efficient bone growth. In other words, the surface of Si_3N_4 encourages

cells to produce bony apatite [8]. Si_3N_4 ceramics also support osteogenesis behaviour where human mesenchymal cells (HMC) differentiate to osteoblast cells [9, 10]. In one study, Si_3N_4 ceramic-based hip prosthesis was compared with the commercially used hip prostheses which are CoCr and Al_2O_3 and it was shown that Si_3N_4 had the lowest artefact level in the MRI images than CoCr and Al_2O_3 [11]. In other studies, Si_3N_4 ceramics were used to investigate the relation between biocompatibility, cell growth behaviour and antibacterial resistance [12, 13]. The Si_3N_4 surface inhibits bacterial colonization because it releases NH_4^+ (in major) and NH_3 (in minor) ions at physiological pH. This

✉ Damion K. Corrigan, damion.corrigan@strath.ac.uk; Fatma D. Güzel, fdogan@ybu.edu.tr | ¹Metallurgical and Materials Engineering Department, Ankara Yildirim Beyazıt University, 06010 Ankara, Turkey. ²Department of Biomedical Engineering, Ankara Yildirim Beyazıt University, 06010 Ankara, Turkey. ³Department of Medical Biochemistry, Faculty of Medicine, Ankara Yildirim Beyazıt University, 06010 Ankara, Turkey. ⁴Department of Biomedical Engineering, University of Strathclyde, Glasgow G1 1XQ, UK. ⁵Department of Metallurgical and Materials Engineering, Eskisehir Osmangazi University, 26040 Eskisehir, Turkey. ⁶Cellular Therapy and Stem Cell Research Center (ESTEM), Eskisehir Osmangazi University, 26040 Eskisehir, Turkey.



SN Applied Sciences (2020) 2:823 | <https://doi.org/10.1007/s42452-020-2624-4>

release occurs due to the covalent bonding of Si–N. The NH_3 ion diffuses into the membrane of the bacteria and reacts with the DNA/RNA, whereas the NH_4^+ ion is used as a nutrient by the cells and induces cells to synthesize proteins to continue the differentiation [12]. Silicon has an important role in osteoblastic activity increment, and nitrogen has an impact on the antibacterial effect. Osteogenic and antibacterial effect of the both Si and N elements and their atomic ratio in Si_3N_4 were also investigated in particular [13]. It was shown that the Si-rich surfaces showed poor osteogenic ability and osteoblast proliferation decreased on its surface. In addition, the important role of nitrogen was investigated in the osteoblast proliferation and osteogenic abilities. To investigate the osteogenic differentiation further, electrochemical impedance spectroscopy (EIS) analysis was used in a different study [14]. The changes in the magnitude of the impedance due to the activity of human mast cell (HMC) used in the study proved that the EIS is a potential candidate cell culture-based in situ analysis technique.

In this study, the cell growth and viability of osteosarcoma cells on the surface of a porous Si_3N_4 substrate were investigated using EIS technique. MG-63 osteosarcoma cells were seeded on the samples, and EIS was used to detect the cell growth by determining its high sensitivity to the changes in the electrode–solution interface of an electrode. Our results confirmed that Si_3N_4 shows promise as a ceramic material in the joint implants, where the integration of bone cells onto the surface is crucial for osseointegration.

2 Materials and methods

2.1 Preparation and physical characterization of samples

$\alpha\text{-Si}_3\text{N}_4$ (UBE SN E10, Japan) and CaO (CaCO_3 , Reidel-de Haen, Germany) were used as starting materials. Powders were mixed by the ball milling process (MSE Technologies, Turkey) at 180 rpm for 24 h by isopropanol alcohol. The powder mix was dried by using rotary evaporation. The tape casting method was chosen for shaping where powder and tape solution (alcohol-based solution) were mixed by a dual asymmetric centrifugal mixer (Speed-Mixer™ (DAC150.1 FVZ)) for 20 min at 3000 rpm. The slurry was casted onto the silicone-coated polyester sheet and shaped by a blade with a thickness of 400 μm . After casting, tape was left to dry to remove all the alcohol-based substances. Tapes were then cut into $15 \times 15 \text{ mm}^2$ square shapes, and 45 samples were laminated. The laminated tapes were pressed by uniaxial press (MSE Technologies, Turkey) under 10 MPa pressure. The polymeric substances

were removed by a burn-out process with the heating rate of 0.5 $^\circ\text{C}/\text{min}$ up to 750 $^\circ\text{C}$. After the burn-out process, sintering was formed at 1700 $^\circ\text{C}$ with a 7 $^\circ\text{C}/\text{h}$ under a nitrogen atmosphere by using an atmosphere controlled furnace (MSE Technologies, Turkey). Dimensions of the samples were reduced into $5 \times 5 \times 5 \text{ mm}^3$ for the cell culture studies. Samples were analysed based on physical characterization in which density, porosity and microstructure were investigated. Density and apparent porosity were measured and calculated by Archimedes' principle. The phase and microstructural analysis were conducted by using XRD (Rigaku Miniflex, Japan) and SEM (Hitachi SU5000, Japan), respectively. The pore sizes and their distribution were analysed by a mercury intrusion porosimetry (Micrometric, Autopore IV, USA).

2.2 Cell culture and cell viability assay

MG-63 osteosarcoma cells were cultured in high-glucose Dulbecco's modified Eagle's medium (DMEM) with 1% L-glutamine, 1% penicillin + streptomycin and 10% foetal bovine serum (FBS). Cells were cultured at 37 $^\circ\text{C}$, 95% humidity and 5% CO_2 until they reached confluence. When cells reached the confluence, they were trypsinated, counted and seeded as 5000 cells/50 μL onto each sample surface. Cell seeded samples were incubated for 4 h to allow cells to attach to the surface in six-well plates, and then 2 mL of fresh medium was slowly added to each well and incubation continued until the first measurement time point. Si_3N_4 samples as the working electrode were then partially submerged in the medium.

WST-1 was used as a measure of cell viability. WST-1 contains a tetrazolium salt which is converted to formazan in the presence of active mitochondrial enzymes. Formazan absorbs light at a wavelength of 440 nm and can therefore be quantified by absorbance measurements at this wavelength. The production of formazan is not toxic to cells, allowing multiple viability measurements to be performed on the same sample. At reading time points, medium from the wells was discarded until only 300–400 μL remained, and then WST-1 was added to a concentration of 10% v/v. Samples were incubated for 3.25 h with WST-1 reagent, then medium containing WST-1 was removed, and finally the absorbance of medium was measured at 440 nm using a microplate reader. Following the medium removal, the wells containing the samples were immediately refilled with the 2 mL fresh DMEM. Control measurements were performed on medium with WST-1 and without WST-1 solutions.

2.3 Electrochemical measurements

EIS was performed using a PalmSens PS4 potentiostat. A 3-electrode cell was used, which consisted of a stainless steel working electrode, counter electrode, and a silver reference electrode. Electrodes were added to the medium where the sample was also immersed (Fig. 1). A 10 mV AC signal was applied on top of a DC bias equal to the open circuit potential (OCP) of the cell, which was measured immediately prior to the measurement being performed. Frequencies were swept from 100 kHz to 0.1 Hz, with 10 steps per decade resulting in 61 measured points. Samples were not removed from the medium during measurements.

Immediately before the addition of the cells to the sample, measurements were taken in fresh medium and the results were used as reference in the EIS analysis. Measurements were then performed in triplicate, with the working electrode being removed and cleaned with 70% isopropyl alcohol between each measurement for the same sample. Alcohol was allowed to fully evaporate before the electrode was replaced in the solution. Between measurements of different samples, all electrodes were removed from the well and then cleaned thoroughly with 70% isopropyl alcohol.

2.4 DAPI staining

Fluorescence staining was performed using DAPI. The presence of cells in the scaffolds was evaluated by fluorescent microscopy at the end of culture period (36 h). After the impedance and WST-1 measurements, scaffolds were washed with sterile phosphate-buffered saline (PBS) and fresh culture medium was added to the scaffolds. The scaffolds were washed with sterile PBS and fixed in 4% neutral formalin. The scaffolds were placed in fluoroshield mounting medium with DAPI solution for 15 min, and transferred on a slide, and examined under a fluorescent microscope (Olympus DP74, Tokyo, Japan) at 20× and 40× magnifications.

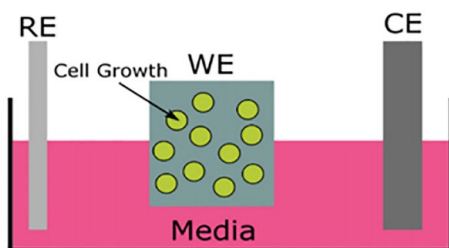


Fig. 1 Schematic of EIS set-up

3 Result and discussion

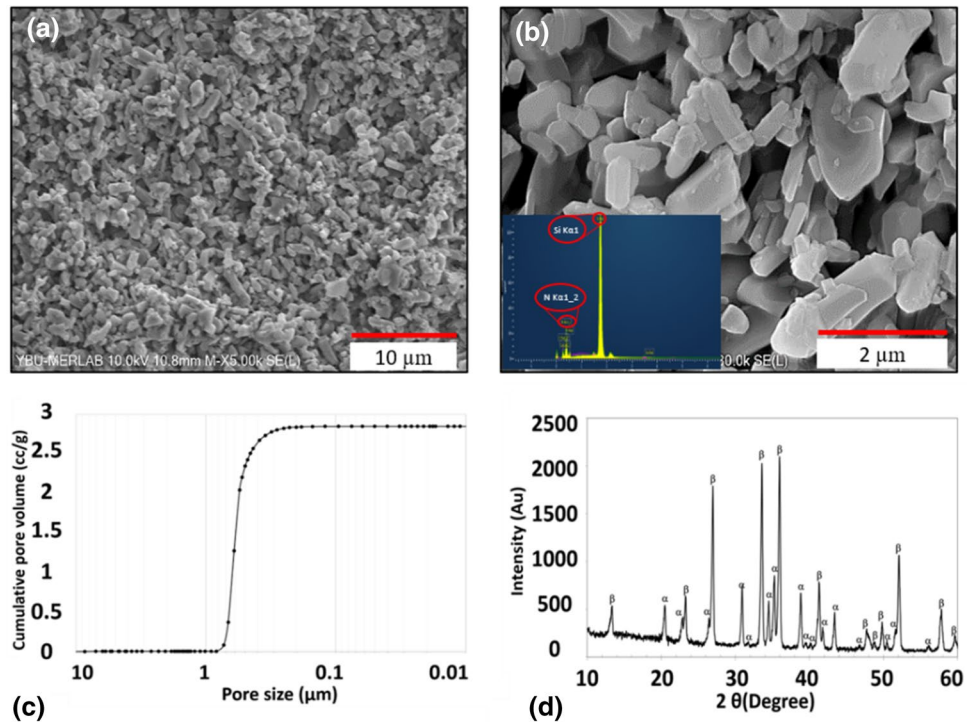
3.1 Material properties

Samples were sintered under partial sintering circumstances by limited temperature (1700 °C) and limited amount of sintering additions. Due to these limitations (sintering time, temperature and amount of sintering aids), a porous structure was obtained. It was shown that mass transport occurs by volume or grain boundary diffusion in Si_3N_4 ceramics in which high amount of covalent bonds causes extremely low diffusion coefficients and this process is activated at high sintering temperatures ~ 1800 °C (for $\alpha\text{-Si}_3\text{N}_4$). When the sintering temperature is lower than ~ 1800 °C, the grain growth cannot complete and porous structure was obtained [15]. The measured bulk density and open porosity were 1.56 g/cm³ and 49.44%, respectively. This type of sintering can be preferable for production of porous ceramics because the technique brings some advantages to the material comparison with other methods such as sacrificial template, replica technique and direct foaming method.

In addition, partial sintering eliminates the need for a special apparatus during sintering of Si_3N_4 ceramics. Fine porous structure of the sample (in Fig. 2a, b) showed that densification was completed, and the bonding of grains occurred via surface diffusion or evaporation–condensation. The structure consisted of both equiaxed and rod-like grains. The lower aspect ratio of the rod-like grains resulted from low sintering temperature. EDX spectrum analysis of the sample, as shown in the inlet of Fig. 2b, confirmed the presence of Si and N as the main component of the sample. Ca and O probably resulted from the sintering additive which have been used in the fabrication procedure.

Mercury intrusion porosimetry was used to estimate the pore size and pore size distribution of the Si_3N_4 . Figure 2c shows the pore size distribution and according to MIP curve, the median pore size was 0.77 μm and mono-modal distribution was obtained. Also, Fig. 2a shows uniform pore sizes that were distributed homogeneously in the microstructure. Instead of formation of rounded pores, irregular-shaped pores were formed as a result of angular shape of Si_3N_4 grains. The XRD pattern (Fig. 2d) of the sample shows that $\beta\text{-Si}_3\text{N}_4$ was formed as a major phase with a minor entity of $\alpha\text{-Si}_3\text{N}_4$. Not only sintering temperature, lower amount of sintering additives also retarded the transformation from α to $\beta\text{-Si}_3\text{N}_4$ by decreasing the amount of liquid phase formed during sintering where transformation occurs via solution and precipitation processes.

Fig. 2 SEM-SE images of Si₃N₄ ceramic at **a** 5000× and **b** 30,000× magnifications, **c** pore size distribution and **d** XRD pattern of Si₃N₄ sample



3.2 Cell viability assay

Figure 3a shows the absorbance of the collected medium following incubation with WST-1 solution for 3.25 h. A higher absorbance shows that a more of the tetrazolium salt was converted by mitochondrial enzymes to formazan. The samples had viable cells present on the surface. WST-1 responses were quite consistent between the time points, but the sample showed a mean increase in cellular activity after 36 h. Moreover, Fig. 3b, c shows fluorescence microscopy images of the sample surfaces following DAPI staining. Typically, the nucleus of MG-63 cells should be rounded and uniform as we observed in Fig. 3b, c.

3.3 Normalized impedance

Impedance data obtained at 20 h and 36 h were normalized against the baseline measurements to visualize how the impedance changed as the cells proliferated and consumed the medium. Normalization was performed according to the following formula [16], which outputs the percentage change from the baseline measurement observed after time *t*;

$$\text{Normalised data}_{(t,f)} = \left(\frac{\text{Data}_{(t,f)}}{\text{Data}_{(0,f)}} - 1 \right) \times 100$$

This normalization was performed on both the impedance magnitude and the phase angle data collected

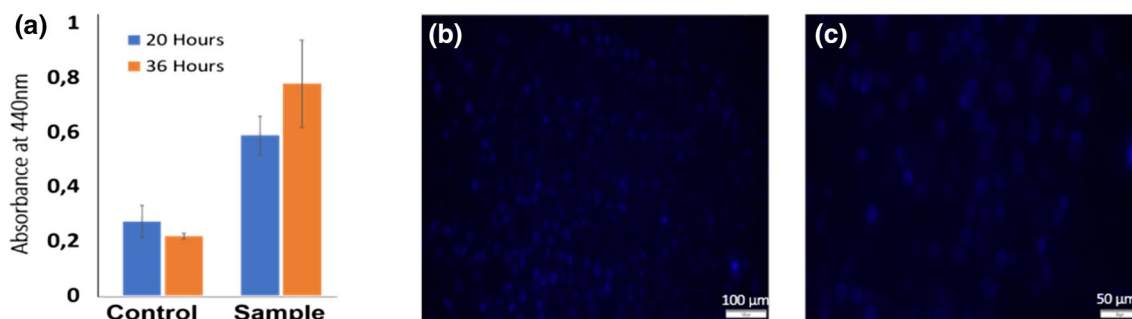


Fig. 3 **a** Spectrophotometer-measured absorbance of medium at 440 nm following 3.25-h sample incubation with WST-1. DAPI staining and fluorescence visualization of cells on substrate after 36 h of growth with **b** 20× and **c** 40× magnifications

during the measurements. The mean of this normalized data was then found and can be seen in Fig. 4.

Within two groups, the phase angle does not show a large change from baseline at any point. There are moderate deviations at high frequencies, but these are typically quite variable with little consistency between samples in the same group. With a higher replicate number, there may be more significant changes in phase angle observed. However, it is currently believed that phase angle is not a reliable indicator of the level of growth of osteosarcoma cells on these samples.

This is to be expected since the impedance measurement employed was probing the cell medium where capacitive effects would have been minimal. Changes in the impedance magnitude appear to be much more consistent as an indicator for cell growth on the sample. The impedance magnitude between 100 kHz and 100 Hz showed a little difference between the different samples at the same time points due to wide standard deviations, but the mean response was quite variable between samples and time points. With increased replicate number, these responses may become more consistent and could possibly show significant differences in cell growth on the sample. The impedance magnitude between 100 Hz and 100 mHz showed similarity between samples and time points. The percentage change in impedance magnitude in this region showed a similar profile in two plots, with the peak impedance change located between 10 and 1 Hz. The percentage change in impedance magnitude is increased ~ 50% in this range. The increase in impedance is likely due to the uptake of charged molecules (salts, amino acids etc.) from the medium by the cells.

Therefore, a greater increase in impedance may reflect the cells growing more effectively on the substrate. Previous work reported in the literature with other cell types (e.g. smooth muscle cells) has shown similar changes in impedance which can be monitored to infer cell behaviour under culture conditions [17] and supports our findings.

Table 1 shows the *p* values from a 2-sample *t* test performed on the normalized impedance magnitude data taken after 36 h. As expected from observation of the graphs, the *p* value at high frequencies is high. As the frequency falls, the *p* values approach 0.05, with a minimum value of 0.101 obtained at 10 Hz. With an increased replicate number, it is believed that statistically significant results could be obtained in the 100–0.1 Hz region.

4 Conclusion

Impedance-based technology is a powerful non-invasive tool to monitor proliferation of adherent cells in culture in the real time. EIS is a label-free, cost effective method enabling the interrogation of living constructs. Once validated, EIS diminishes the need to use histological and biochemical assays to evaluate viability, proliferation and cell differentiation which are also time-consuming and expensive techniques. The results presented here show that osteosarcoma cells will successfully colonize onto a silicon nitride sample, and this colonization is semi-quantitatively detectable using EIS measurements of the cell medium as discussed in our study. EIS results correlated well with the DAPI staining tests indicating that cells are growing on the

Fig. 4 Mean normalized impedance magnitude and phase angle measured from Si_3N_4 samples, 20 h (left) and 36 h (right) after initial inoculation on substrate. $N=3$. Shading shows standard deviation

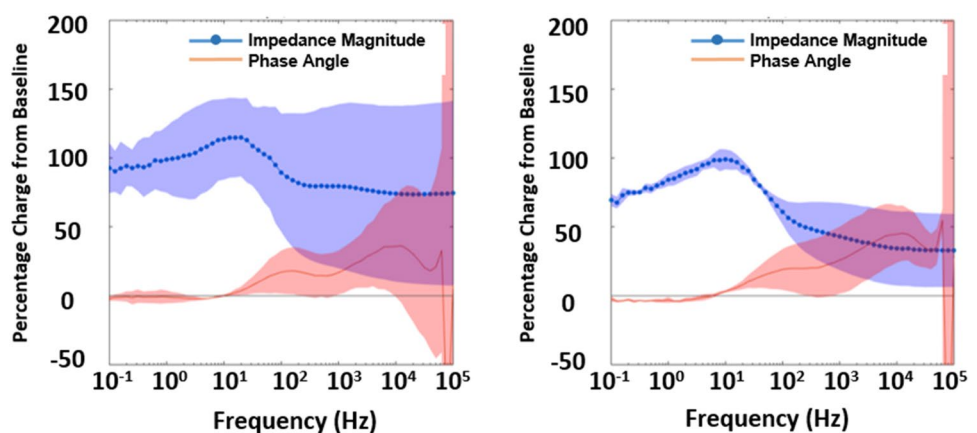


Table 1 Results from 2-sample *t* test performed on normalized impedance magnitude (*Z*) data from 36 h trial

Frequency (Hz)	100,000	10,000	1000	100	10	1	0.1
<i>P</i> value	0.601	0.607	0.729	0.495	0.101	0.141	0.151

sample. WST-1 results showed an increase in cell growth in correlation with EIS and histology findings.

The experiment performed here is not representative of an impedimetric sensor attached directly to a silicon nitride sample. However, it shows the changes in the biological activity of the cell-culturing medium and thus indirectly represents the biocompatibility of Si_3N_4 . In conclusion, the sensitivity of EIS can be a criterion to obtain useful information on cell growth and viability; however, further studies are required to establish more quantitative relationship.

Acknowledgements Authors would like to acknowledge Scientific Research Projects Funds (BAP - 4116) from Ankara Yildirim Beyazit University for the support of this study. DC and AB would like to thank the Scottish Funding Council (SFC) for award of a pump-priming grant to enable this collaboration.

Funding This study was funded by Scientific Research Projects Funds (BAP - 4116), Ankara Yildirim Beyazit University and the Scottish Funding Council (SFC).

Compliance with ethical standards

Conflict of interest The corresponding author states that there is no conflict of interest.

Open Access This article is licensed under a Creative Commons Attribution 4.0 International License, which permits use, sharing, adaptation, distribution and reproduction in any medium or format, as long as you give appropriate credit to the original author(s) and the source, provide a link to the Creative Commons licence, and indicate if changes were made. The images or other third party material in this article are included in the article's Creative Commons licence, unless indicated otherwise in a credit line to the material. If material is not included in the article's Creative Commons licence and your intended use is not permitted by statutory regulation or exceeds the permitted use, you will need to obtain permission directly from the copyright holder. To view a copy of this licence, visit <http://creativecommons.org/licenses/by/4.0/>.

References

- Bal BS, Rahaman MN (2012) Orthopedic applications of silicon nitride ceramics. *Acta Biomater* 8(8):2889–2898
- Güzel FD, Miles B (2018) Development of in-flow label-free single molecule sensors using planar solid-state nanopore integrated microfluidic devices. *Micro Nano Lett* 13(9):1352–1357
- Cabeza LV (1974) Dosimetry of the SIN biomedical pion beam with tissue-equivalent ionization chambers. In: *RöFo-Fortschritte auf dem Gebiet der Röntgenstrahlen und der bildgebenden Verfahren*, 1974. vol 07. © Georg Thieme Verlag KG Stuttgart, New York, pp 109–114
- Lin S, Shi S, LeGeros RZ, LeGeros JP (2000) Three-dimensional finite element analyses of four designs of a high-strength silicon nitride implant. *Implant Dent* 9(1):53–60

- Silva CG, Higa O, Bressiani JC (2004) Cytotoxic evaluation of silicon nitride-based ceramics. *Mater Sci Eng C* 24(5):643–646
- Silva CG, König B Jr, Carbonari M, Yoshimoto M, Allegrini S Jr, Bressiani JC (2008) Bone growth around silicon nitride implants—an evaluation by scanning electron microscopy. *Mater Charact* 59(9):1339–1341
- Guedes e Silva CC, König B Jr, Carbonari MJ, Yoshimoto M, Allegrini S Jr, Bressiani JC (2008) Tissue response around silicon nitride implants in rabbits. *J Biomed Mater Res Part A* 84(2):337–343
- Pezzotti G, Oba N, Zhu W, Marin E, Rondinella A, Boschetto F, McEntire B, Yamamoto K, Bal BS (2017) Human osteoblasts grow transitional Si/N apatite in quickly osteointegrated Si_3N_4 cervical insert. *Acta Biomater* 64:411–420
- Howlett C, McCartney E, Ching W (1989) The effect of silicon nitride ceramic on rabbit skeletal cells and tissue. An in vitro and in vivo investigation. *Clin Orthop Relat Res* 244:293–304
- Pezzotti G, McEntire BJ, Bock R, Boffelli M, Zhu W, Vitale E, Puppulin L, Adachi T, Yamamoto T, Kanamura N, Bal BS (2016) Silicon nitride: a synthetic mineral for vertebrate biology. *Sci Rep* 6(1):1–7
- Rodrigues SP, Paiva JM, De Francesco S, Amaral MI, Oliveira FJ, Silva RF (2013) Artifact level produced by different femoral head prostheses in CT imaging: diamond coated silicon nitride as total hip replacement material. *J Mater Sci Mater Med* 24(1):231–239
- Zanocco M, Boschetto F, Zhu W, Marin E, McEntire BJ, Bal BS, Adachi T, Yamamoto T, Kanamura N, Ohgitani E, Yamamoto K (2020) 3D-additive deposition of an antibacterial and osteogenic silicon nitride coating on orthopaedic titanium substrate. *J Mech Behav Biomed Mater* 103:103557
- Zanocco M, Marin E, Rondinella A, Boschetto F, Horiguchi S, Zhu W, McEntire BJ, Bock RM, Bal BS, Pezzotti G (2019) The role of nitrogen off-stoichiometry in the osteogenic behavior of silicon nitride bioceramics. *Mater Sci Eng C* 105:110053
- Hildebrandt C, Büth H, Cho S, Thielecke H (2010) Detection of the osteogenic differentiation of mesenchymal stem cells in 2D and 3D cultures by electrochemical impedance spectroscopy. *J Biotechnol* 148(1):83–90
- Kalemtas A, Topates G, Özcoban H, Mandal H, Kara F, Janssen R (2013) Mechanical characterization of highly porous $\beta\text{-Si}_3\text{N}_4$ ceramics fabricated via partial sintering & starch addition. *J Eur Ceram Soc* 33(9):1507–1515
- Meijs S, Fjorback M, Sørensen S, Rechendorff K, Rijkhoff NJ (2014) Increasing voltage transients using implanted titanium nitride neural stimulation electrodes. Replace, repair, restore, relieve—bridging clinical and engineering solutions in neurorehabilitation. Springer, Berlin, pp 543–551
- Holland I, McCormick C, Connolly P (2018) Towards non-invasive characterisation of coronary stent re-endothelialisation—an in-vitro, electrical impedance study. *PLoS One* 13(11):1–17

Publisher's Note Springer Nature remains neutral with regard to jurisdictional claims in published maps and institutional affiliations.